Influence of the initial Li/Co ration in LiCoO2 on the high-voltage phase-transition mechanisms

Marie Duffiet, Maxime Blangero, Pierre-Etienne Cabelguen, Claude Delmas, Dany Carlier

Influence of the Initial Li/Co Ratio in $LiCoO_2$ on the High Voltage Phase Transitions Mechanisms

Marie Duffiet[1,2], *Maxime Blangero*[2], *Pierre-Etienne Cabelguen*[3], *Claude Delmas*[1], *Dany Carlier*[1*]

[1] CNRS, Univ. Bordeaux, Bordeaux INP, ICMCB UMR 5026, F-33600 Pessac, France

[2] Umicore, Materials Research and Development, Cheonan-Shi, Chungnam-Do 330-200, Korea

[3] Umicore Rechargeable battery materials, 31 rue du marais, Brussels BE-1000, Belgium

* Corresponding author: dany.carlier@icmcb.cnrs.fr

The influence of the initial Li/Co stoichiometry in $LiCoO_2$ (LCO) ($1.00 \leq Li/Co \leq 1.05$) on the phase transition mechanisms occurring at high voltage during lithium de-intercalation ($V > 4.5$ *vs.* Li^+/Li) was investigated by *in situ* X-ray diffraction. Even if the excess Li^+ in $Li_{1.024}Co_{0.976}O_{1.976}$ doesn't hinder the formation of the H1-3 and O1 phases, the latter are obtained at higher voltages and exhibit larger *c* parameters compared to their analogues formed from $Li_{1.00}CoO_2$. We also showed that for the stoichiometric $Li_{1.00}CoO_2$, the de-intercalation process is more complex than already reported, with the formation of an intermediate structure between H1-3 and O1.

TOC Graphic:

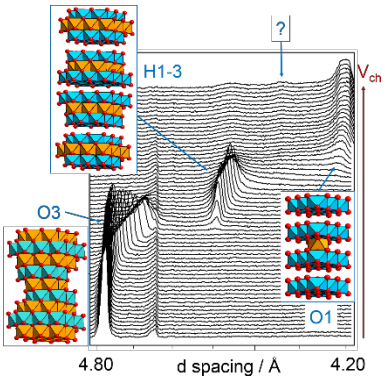

Layered $LiCoO_2$ (LCO) crystallizing in the R-3m space group has been extensively studied for years as positive electrode material for Li-ion batteries (LiBs) since its discovery by Goodenough[1]. Still today, it is one of the most common materials in commercial LiBs used in portable electronics, thanks to its great ability to reversibly de-intercalate and re-intercalate lithium over thousands of cycles up to 4.3 V *vs.* Li^+/Li (equivalent to 4.2 V *vs.* graphite). Up to this voltage, approximately x = 0.62 Li can be extracted corresponding to a charge capacity of about 174 mAh/g *vs.* Li^+/Li.

Li^+ ions removal is accompanied by an insulator – metal transition[2] occurring at 3.95 V leading to a biphasic domain followed by a reversible structural change from a rhombohedral to a monoclinic phase (O3 → O'3) observed at x = 0.5 due to Li^+/vacancy ordering[3,4]. Both phenomena can be clearly identified on the $LiCoO_2$//Li electrochemical cycling curve and have contributed to make it a very typical signature of the stoichiometric $LiCoO_2$ (noted st-LCO in the following). In fact, as shown by Levasseur, st-LCO is the end member of a $Li_1[Li_tCo_{1-t}]O_{2-t}$ solid solution where extra lithium ions occupy the cobalt site; the electrical neutrality being insured by oxygen vacancies[5]. The material prepared with Li/Co > 1.00 will be called overlithiated $LiCoO_2$ (noted overl-LCO in the following) (Supporting information-S1). Even if the solid solution range is very narrow t < 0.04, the effect on the electrochemical behavior is significant *vs.* st-LCO; as a result of the Li-excess defects and entropy increase, the two-phase domain and the monoclinic distortion disappear while cycling at room temperature. The presence of oxygen vacancies leads to the formation of intermediate spin Co^{3+} which are indirectly detected by ^7Li NMR, making this technique the best way to characterize Li-overstoichiometry[5,6].

Increasing the charge voltage higher than 4.3 V *vs.* Li^+/Li would enable the extraction of more Li^+ ions and reach charge capacities higher than 174 mAh/g. In this state of charge range, a

dramatic degradation of cycling performance prevents industrial applications. In particular, structural transitions and electronic evolutions at such high voltages are believed to be root causes of material degradation and cell failure (electrolyte oxidation and oxygen loss on the particle surface, cobalt dissolution resulting in destabilization of anode SEI, particle fracturing and loss of electrical contact…). In the last years, many strategies have been explored to overcome these issues, by either: i) slightly tuning the initial chemical composition of LCO with the substitution of some Co^{3+} ions with many different dopants such as Mg, Ti or Al[7–10], or ii) changing the surface composition of the LCO particles, coating metal oxides[11,12], fluorides[13,14], phosphates[15] and carbonates[16]. In the meantime, least attention has been given to a more fundamental knowledge about the mechanisms of structural changes in the LCO system. Even if a few articles[17–20] have identified two major topotactic phase transitions from O3 → H1-3 → O1 structures occurring above 4.4 V *vs.* Li^+/Li, the possible influence of the initial Li/Co stoichiometry on those mechanisms has not been investigated yet. In this paper, we aim to better evidence the structural transitions occurring at high voltage depending on the Li/Co stoichiometry of the pristine LCO phase and particle size. ^{7}Li magic angle spinning nuclear magnetic resonance spectroscopy (^{7}Li MAS NMR) was used to properly assess the Li/Co stoichiometry of the samples. *In situ operando* X-ray diffraction was used to characterize the structural transitions occurring at high voltage (up to 5 V).

In a preliminary study we demonstrated that the particle size of the LCO materials in the *µm* range (2 - 4 *µm* vs 10 - 30 *µm*) did not affect the phase transition mechanisms occurring at high voltage (Supporting information S2). We will thus focus the discussion here on the impact of the initial lithium content x_0 (correlated to the initial Li/Co stoichiometry, as $Li/Co = (1+t)/(1-t) = x_0 / (1-t)$). We selected two samples: (i) a stoichiometric $LiCoO_2$ (denoted as

"st-LCO") with Li/Co = 0.99 and D_{50} = 34 µm, (ii) an overlithiated $Li_{1.024}Co_{0.976}O_{1.976}$ (denoted as "overl-LCO") with Li/Co = 1.05 and D_{50} = 15 µm. General characterization of the two samples is provided in Supporting Information (Figure S3). The layered structure of st-LCO and overl-LCO is confirmed by the XRD patterns (both indexed in the *R-3m* space group). Additionally, traces of Co_3O_4 are detected for st-LCO, as expected for a sample prepared with an initial Li/Co ratio of 0.99. No clear change of cell parameters can be observed depending on the initial Li/Co stoichiometry of the two samples. Substantial differences between st-LCO and overl-LCO can only be found in their ^{7}Li MAS NMR spectra. Indeed, the ^{7}Li MAS NMR spectrum for st-LCO shows a single diamagnetic signal centered at -0.4 ppm, while several more signals are detected for overl-LCO. This is a clear confirmation that st-LCO is, indeed, stoichiometric, as its only signal arises from the presence of a low spin state diamagnetic (LS) Co^{3+} environment. The additional signals observed for overl-LCO – whose exact assignation is still unknown – are though confirming the presence of paramagnetic intermediate spin IS-Co^{3+} cobalt ions formed due to the presence of Li in the Co site associated with an O vacancy[5,6]. As these differences have already proven to significantly change the electrochemical behavior of LCO samples, the corresponding electrochemical cycling curves obtained using the two LCO samples *vs.* Li in coin cells cycled in the 3.0 - 4.7 V and 3.0 - 5.0 V voltage ranges are provided in Figure 1. As already reported, the two samples exhibit different shape in the low voltage domain (no plateau at 3.95 V and no phase transition at x = 0.5 for overl-LCO). In the high voltage domain up to 4.7 V the profiles differ: i) upon charge, a small plateau can be observed at 4.53 V for st-LCO, well evidenced by the narrow and intense peak on the dx/dV curve, whereas a broader contribution is observed for such potential for overl-LCO; ii) upon discharge from 4.7 V, st-LCO sample does clearly exhibit two successive plateaus at 4.52 V and 4.48 V, whereas overl-LCO exhibits only one plateau at 4.45 V. A larger irreversible capacity loss is systematically observed for overl-LCO independently of the applied

cut off voltage. Last and for both samples, a large polarization is observed when the batteries are cycled up to 5 V.

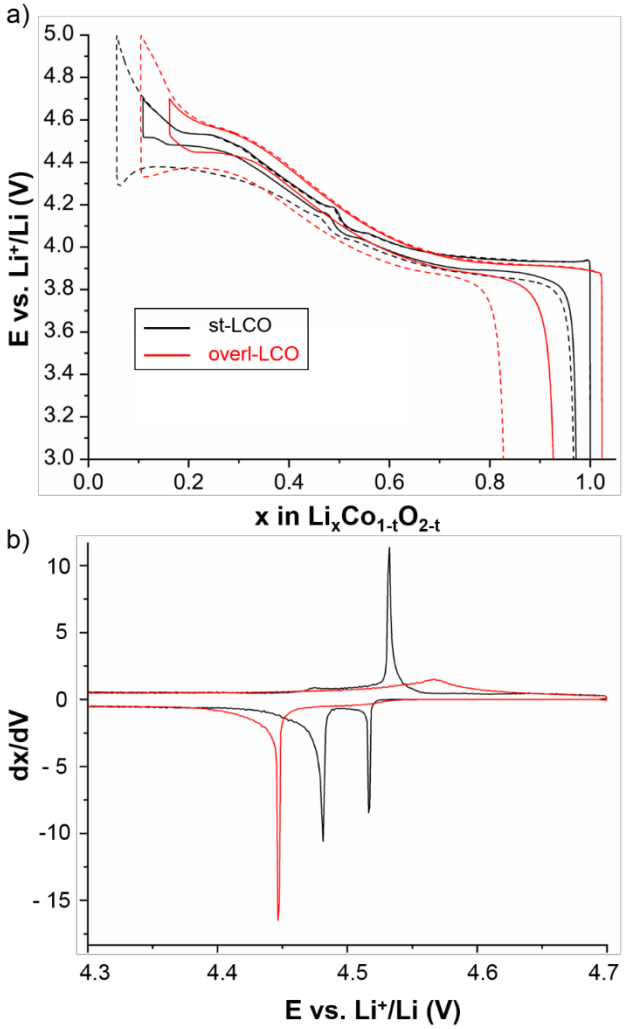

Figure 1. 1st cycle for st-LCO (x_0 = 1.00) and overl-LCO (x_0 = 1.024) at C/30 as positive electrode in Li//LCO cells at two cutoff voltages (4.7 V and 5.0 V) (a). Associated dx/dV curves for the high voltage window 4.3 - 5.0 V (b).

In order to better understand those phenomena, we recorded *in situ operando* XRD patterns in the high voltage range for both LCO samples. In Figure 2, we plotted the patterns collected for

the most intense (0 0 ℓ) diffraction line upon charge in two relevant voltage domains for more clarity: 4.20 - 4.60 V (a, b) and 4.55 - 5.0 V (c,d), respectively corresponding to the successive O3 – H1-3 and H1-3 – O1 phase transitions already reported in the literature for supposedly Li-stoichiometric samples only[20,21]. For a better understanding of the mechanisms, we also plotted the evolution of the $d_{(0\,0\,\ell)}$ interslab spacing as a function of the voltage in Figure 3. At ~ 4.20 V vs Li^+/Li, the two compounds exhibit a single sharp intense diffraction line, corresponding to the (0 0 3) diffraction peak of a O3-type Li_xCoO_2 structure with a similar interslab distance for the two materials ($d_{(0\,0\,3)}$ = 4.81 Å), higher than the one of the pristine materials ($d_{(0\,0\,3)}$ = 4.68 Å). At 4.20 V vs Li^+/Li, approximately 0.4 Li^+ ions are remaining in both LCO compounds. A schematic representation of the O3 structure is given in Figure 3. As we slowly further de-intercalate Li^+ ions up to 4.55 V, the interlayer distance $d_{(0\,0\,3)}$ decreases as revealed by the shift of peak position on Fig. 2a and 2b. This signal also undergoes a clear broadening assigned to the competition between nucleation and growth of O1-type stacking faults into the O3-type matrix. No other significant change is observed for this $(0\,0\,3)_{O3}$ peak before the appearance of a new peak at 4.53 V and at 4.57 V for st-LCO and overl-LCO, respectively. This peak corresponds to the (0 0 6) diffraction line of the H1-3-type structure (depicted in Figure 3). For st-LCO, the associated average interlayer distance $d_{(0\,0\,6)}$ is 4.51 Å, meaning that the corresponding $c_{hex.}$ parameter is approximately 27.06 Å, in good agreement with the value reported by Dahn's group[20] (27.07 Å). Despite the presence of defects in the pristine overl-LCO, the H1-3 phase is formed during Li^+ de-intercalation but appears at slightly higher voltage and does exhibit a higher interlayer distance ($d_{(0\,0\,6)}$ = 4.55 Å). The slab distance range observed for the intermediate H1-3 phase is also different for the two compounds: very narrow for st-LCO (d varies between 4.51 Å and 4.46 Å) and larger for overl-LCO (d varies between 4.55 to 4.45 Å).

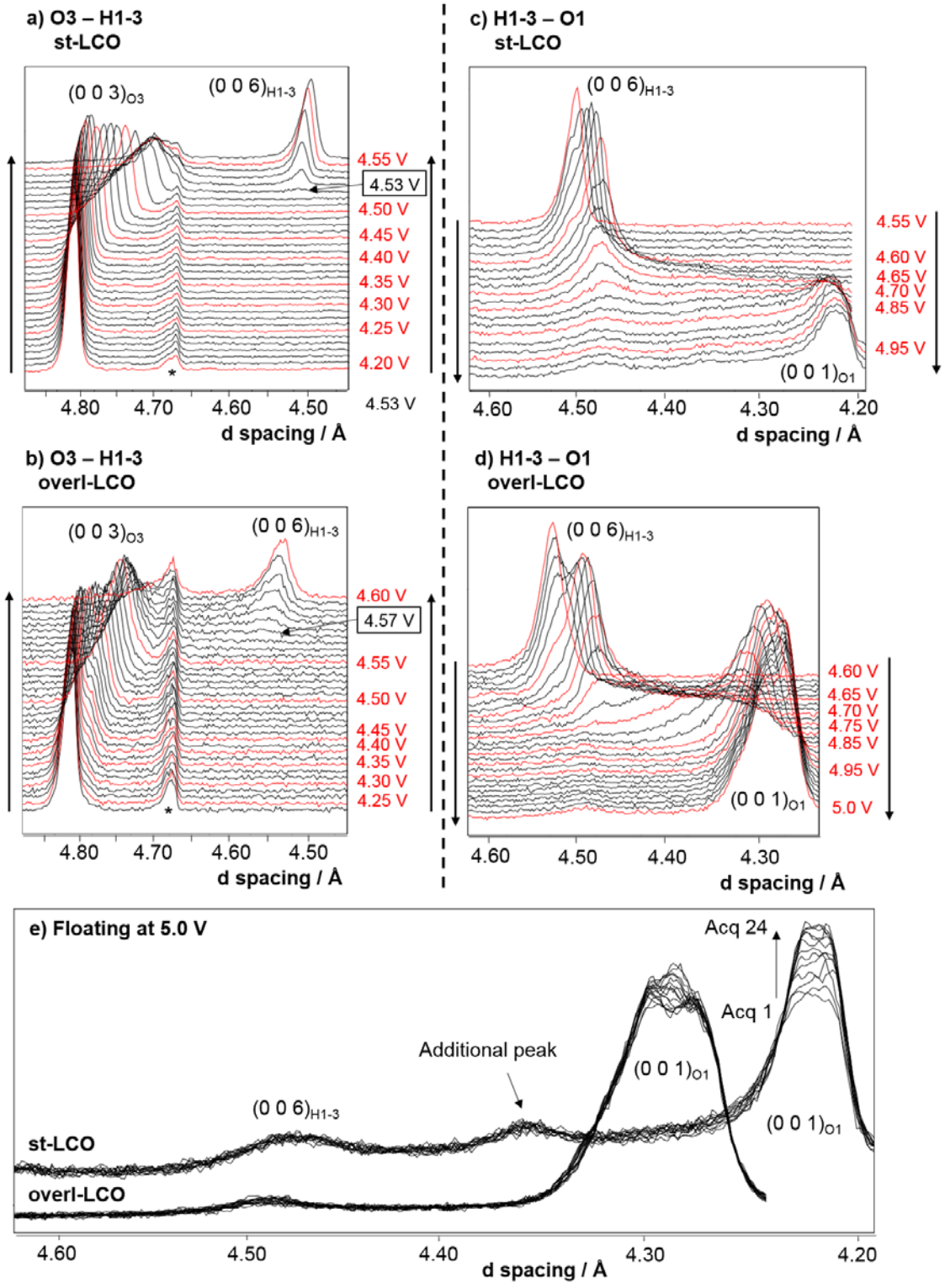

Figure 2. [2 columns] Cumulated XRD patterns recorded *in situ operando* during the charge of st-LCO and overl-LCO, plotted as a function of $d_{(00l)}$ spacing in the 4.20 – 4.55V (or 4.60 V) vs. Li^+/Li voltage range (a,

b) and in the 4.55 (or 4.60 V) - 5.00 V (c, d) range, respectively corresponding to the successive O3 – H1-3 and H1-3 – O1 phase transitions. The black arrows show the evolution of the patterns towards the charge. Figure (e) is dedicated to a comparison of patterns obtained at the very end of the charge, as we maintained a constant potential reaching E = 5.0 V. The peak identified with (*) is a line from the cell.

Upon further charge up to 5 V, the mechanism observed for the two materials are clearly different (Figure 2c and d). For st-LCO, whereas a single transition from H1-3 to O1 structural type is expected from literature[18,20,21], we first observe a gradual broadening and asymmetry of the $(0\ 0\ 6)_{H1\text{-}3}$ diffraction line towards the lower d values, then the appearance of two new "diffraction lines" corresponding to d = 4.36 Å and 4.23 Å, both still very broad. The line at 4.23 Å can be assigned to the (0 0 1) diffraction line of the O1 structure type already reported in the 1990's by Amatucci *et. al*[18], but the line located at 4.36 Å was not reported so far and might result from intergrowth between H1-3 and O1 structures. The appearance of the new peak at 4.36 Å is better seen on the XRD pattern, after we applied a potentiostatic step at E = 5.0 V for several hours following the charge of the compound and recorded a few more patterns (Figure 2e). Since it is located for intermediate d-values between H1-3 and O1 phases, we propose that the intergrowth between these structures is not completely random, thus forming an intermediate stacking. Its formation could be a way to minimize the internal constraints due to the strong d-interslab space diminution from H1-3 to O1 for the system. Note that even after a long floating at 5 V, the diffraction lines for the three phases (H1-3, intermediate and O1) are still observed (Fig. 2e). In any case, from their peak broadening, those structures may contain a high number of stacking faults resulting in overall structural disorder. For overl-LCO, the mechanism is different, no intermediate peak is observed: the H1-3 structure gradually transform into an O1 structure with the formation of several intermediate stacking faulted structures, with a continuous process.

In addition, it can be noticed that the final O1 structures obtained from both st-$LiCoO_2$ and overl-$LiCoO_2$ show significant differences regarding their respective interslab spacing. Indeed, a lower value for st-LCO (d_{001} = 4.23 Å) sample is obtained, as compared to overl-LCO (d_{001} = 4.31 Å) sample. This could be related to the presence of vacancies in the $Co_{1-t}O_{2-t}$ slabs.

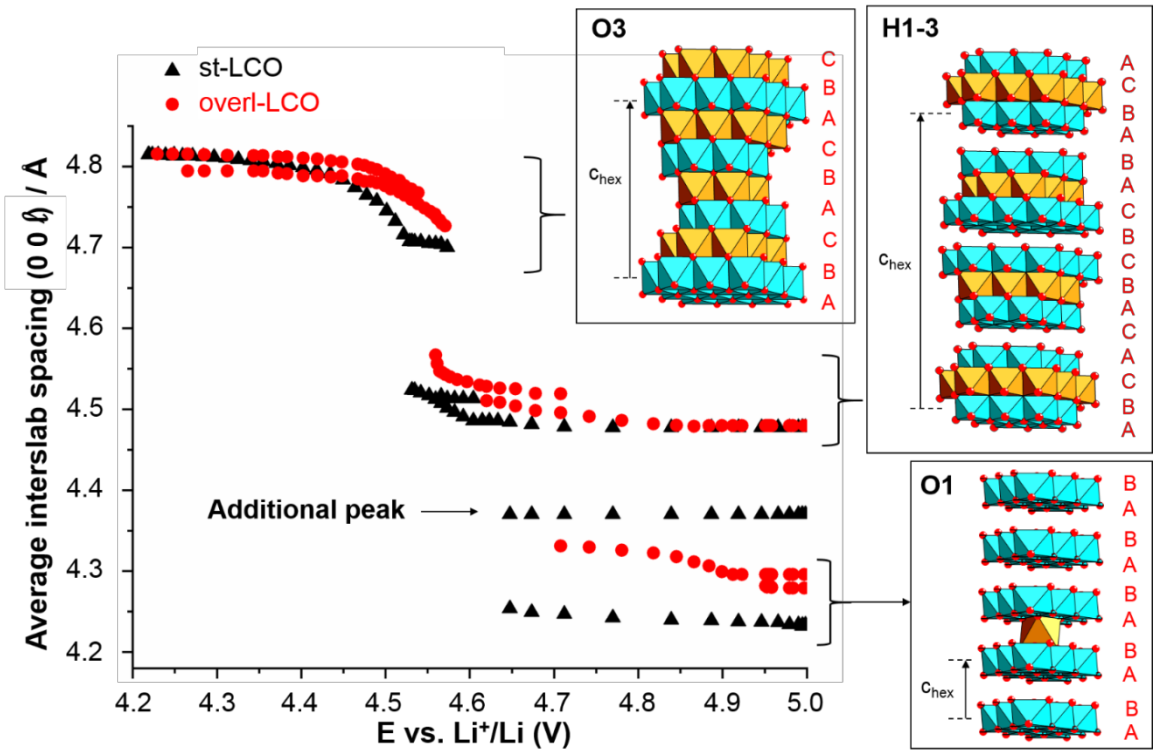

Figure 3. [2 columns] Plot of the average interlayer distance d(0 0 ℓ) for each phase formed during the charge of st-LCO and overl-LCO as function of E *vs.* Li^+/Li. The values for d(0 0 ℓ) are reported for each XRD pattern shown in Figure 2. For better understanding, structures for all phases are schematically depicted in small boxes, on the right of the figure. The blue octahedra are CoO_6 units, while the yellow ones are possible LiO_6. Letters in red represent the oxygen stacking, each letter corresponding to an oxygen position as followed: A (0 0 z_A); B (⅓ ⅔ z_B); C (⅔ ⅓ z_C).

Following the conclusions on the effect of the initial Li/Co stoichiometry on Li^+ de-intercalation process at low voltage (below 4.4 V) for LCO materials, we showed that the initial

Li/Co stoichiometry also affect the mechanisms involved at high voltage. The successive structural transitions from O3 to H1-3 and O1 phase are observed for both samples, but these phases appear at higher voltage and does exhibit different cell parameters for an overlithiated compound. Note that less volume changes are obtained for the overlithiated compound despite a higher irreversible capacity, that may therefore be due to some structural reorganization, stronger electrolyte oxidation and cobalt dissolution. We also showed that for the stoichiometric LCO, the de-intercalation process occurring at high voltage is more complex than already reported, with the formation of an intermediate phase between H1-3 and O1. Further investigation using synchrotron XRD will be required to better understand those phenomena.

Experimental methods

Different LCO samples were provided by Umicore with various Li/Co stoichiometries and particle sizes.

Powder X-ray diffraction (XRD) patterns were collected on a PANalitycal X'pert PRO MPD diffractometer in Bragg-Brentano θ-θ geometry equipped with a Fe filter, a spinner and X'Celerator multi-strip detector. Each measurement was made within an angular range of 2θ = 10 - 120° and lasted for 15 hours with 0.016° intervals. The Co-Kα radiation was generated at 35 kV and 30 mA ($\lambda(K_{\alpha 1})$ = 1.789 Å; $\lambda(K_{\alpha 2})$ = 1.793 Å).

^{7}Li MAS NMR spectra were recorded on a Bruker 300 Avance spectrometer at 116 MHz (7.05 T magnet), with a standard 2.5 mm Bruker MAS probe. A Hahn echo sequence [$t_{\pi/2}$-τ1-t_{π}-τ2] synchronized with one period of rotor rotation was used for a 30 kHz spinning frequency. The 90° pulse duration was equal to $t_{\pi/2}$ = 2.0 μs was determined using a LiCl 1 M solution. A recycle time of D_0 = 40 s was used for st-LCO, whereas a shorter D_0 = 2s was enough for the overl-LCO sample, to avoid T1 saturation effects.

Scanning electron micrographs (SEM) were taken using a Hitachi Model S-4500 microscope after metallizing the powders with gold.

For BET (Brunauer, Emmett et Teller) measurements, we used Micromeritics, TriStar II 3020 equipment. A nitrogen gas was applied for sample flushing at 300℃ for 1 h and helium gas for measurement at 25℃.

Inductively Coupled Plasma (ICP) measurements were carried out on Agilent ICP-720ES equipment after sample digestion using hotplate heating in concentrated HCl solution. A "4-point" method was used.

LCO:C:PVDF electrodes (90:5:5 $\%_{wt}$) with the two above-mentioned LCO active materials were prepared from a slurry using N-methyl-pyrrolidone (NMP) as solvent casted onto 6.5µm-thick-aluminum circles for the *in situ* XRD experiments. Typical active material loading and diameter for an electrode used during *in situ* XRD experiments were respectively 15 mg/cm² and 20 mm; 10mg/cm² and 15mm for tests in coin cells. The electrodes were dried overnight under vacuum at T = 120 °C and stored in an argon-filled glovebox, the homemade *in situ* cells were assembled using pure lithium as counter-electrode and 1 M $LiPF_6$ in EC:DEC:DMC as electrolyte. Coin cells for preliminary tests were assembled the same way.

For the *in situ* XRD experiments, electrodes were pre-charged at C/30 up to 4.2 V without collecting any XRD pattern, since the goal of this experiment was the investigation of the phase transitions occurring at higher voltage. After reaching E = 4.2 V *vs.* Li^+/Li, the charge proceeded at a lower C rate C/100 up to 5.0 V. XRD patterns were collected *in operando* on a PANalytical X'Pert PRO MPD diffractometer, using the Cu $K\alpha_1$ radiation. Special attention was given to the (0 0 ℓ) diffraction peak evolution, that allows to directly follow the changes in the interslab distance which is characteristic of the metal and lithium layer stacking modifications. Therefore, XRD acquisition was recorded every hour between 18 and 21.6°. Due to large exposure time at high voltages leading to substantial electrolyte degradation, we chose to discuss the data versus the cell voltage in the following and not versus state of charge expressed by the lithium amount (x). As a composition guide line, the formula of the ideal H1-3 phase is $Li_{0.167}CoO_2$ while the O1 phase is expected for the CoO_2 composition.

Acknowledgements

This work beneficiates from financial support from Umicore within the framework of Conventions Industrielles de Formation par la REcherche (CIFRE), handled by the Association Nationale Recherche Technologie (ANRT). We would like to thank them to this end. We are also grateful to Laurent Gautier and Stéphane Levasseur (Umicore) for fruitful discussions. Michel Ménétrier and Cathy Denage's involvements in the ^{7}Li MAS NMR and SEM were greatly appreciated too.

Supporting information:

The Supporting Information is available free of charge on the ACS Publications website.

Schematic structures of the st-LCO and overl-LCO materials are providing in S1. In S2, data for st-LCO with different particles size are compared and in S3 complementary data for st-LCO and overl-LCO are provided.

References

(1) Mizushima, K.; Jones, P. C.; Wiseman, P. J.; Goodenough, J. B. Li_xCoO_2 ($0 < x < 1$): A New Cathode Material for Batteries of High Energy Density. *Mater. Res. Bull.* **1980**, *15* (6), 783–789.

(2) Ménétrier, M.; Saadoune, I.; Levasseur, S.; Delmas, C. The Insulator-Metal Transition upon Lithium Deintercalation from $LiCoO_2$: Electronic Properties and ^{7}Li NMR Study. *J. Mater. Chem.* **1999**, *9* (5), 1135–1140.

(3) Shao-Horn, Y.; Levasseur, S.; Weill, F.; Delmas, C. Probing Lithium and Vacancy Ordering in O3 Layered Li_xCoO_2 ($x \approx 0.5$) An Electron Diffraction Study. *J. Electrochem. Soc.* **2003**, *150* (3), A366–A373.

(4) Reimers, J. N.; Dahn, J. R. Electrochemical and In Situ X-Ray Diffraction Studies of Lithium Intercalation in Li_xCoO_2. *J. Electrochem. Soc.* **1992**, *139* (8), 2091–2097.

(5) Levasseur, S.; Ménétrier, M.; Shao-Horn, Y.; Gautier, L.; Audemer, A.; Demazeau, G.; Largeteau, A.; Delmas, C. Oxygen Vacancies and Intermediate Spin Trivalent Cobalt Ions in Lithium-Overstoichiometric $LiCoO_2$. *Chem. Mater.* **2003**, *15* (1), 348–354.

(6) Ménétrier, M.; Carlier, D.; Blangero, M.; Delmas, C. On "Really" Stoichiometric $LiCoO_2$. *Electrochem. Solid-State Lett.* **2008**, *11* (11), A179–A182.

(7) Myung, S.-T.; Kumagai, N.; Komaba, S.; Chung, H.-T. Effects of Al Doping on the Microstructure of $LiCoO_2$ Cathode Materials. *Solid State Ion.* **2001**, *139* (1–2), 47–56.

(8) Yu, J.; Han, Z.; Hu, X.; Zhan, H.; Zhou, Y.; Liu, X. The Investigation of Ti-Modified $LiCoO_2$ Materials for Lithium Ion Battery. *J. Power Sources* **2014**, *262*, 136–139.

(9) Prahasini, P.; Sivakumar, M.; Subadevi, R.; Wang, F. M. Synthesis and Characterization of Cu Doped $LiCoO_2$ Cathode Material for Lithium Batteries Using Microwave Assisted Sol-Gel Synthesis. *Adv. Mater. Res.* **2012**, *584*, 345–349.

(10) Liu, A.; Li, J.; Shunmugasundaram, R.; Dahn, J. R. Synthesis of Mg and Mn Doped $LiCoO_2$ and Effects on High Voltage Cycling. *J. Electrochem. Soc.* **2017**, *164* (7), A1655–A1664.

(11) Kim, Y. J.; Cho, J.; Kim, T.-J.; Park, B. Suppression of Cobalt Dissolution from the $LiCoO_2$ Cathodes with Various Metal-Oxide Coatings http://jes.ecsdl.org/content/150/12/A1723 (accessed Mar 1, 2018).

(12) Cho, J.; Kim, Y. J.; Kim, T.-J.; Park, B. Zero-Strain Intercalation Cathode for Rechargeable Li-Ion Cell. *Angew. Chem.* **2001**, *113* (18), 3471–3473.

(13) Sun, Y.-K.; Yoon, C. S.; Myung, S.-T.; Belharouak, I.; Amine, K. Role of AlF_3 Coating on $LiCoO_2$ Particles during Cycling to Cutoff Voltage above 4.5 V. *J. Electrochem. Soc.* **2009**, *156* (12), A1005–A1010.

(14) Lee, H. Jin; Park, Y. J. Interface Characterization of MgF_2-Coated $LiCoO_2$ Thin Films. *Solid State Ion.* **2013**, *230*, 86–91.

(15) Kim, J.; Noh, M.; Cho, J.; Kim, H.; Kim, K.-B. Controlled Nanoparticle Metal Phosphates (Metal = Al , Fe, Ce, and Sr) Coatings on $LiCoO_2$ Cathode Materials. *J. Electrochem. Soc.* **2005**, *152* (6), A1142–A1148.

(16) Dai, X.; Zhou, A.; Xu, J.; Lu, Y.; Wang, L.; Fan, C.; Li, J. Extending the High-Voltage Capacity of $LiCoO_2$ Cathode by Direct Coating of the Composite Electrode with Li_2CO_3 via Magnetron Sputtering. *J. Phys. Chem. C* **2016**, *120* (1), 422–430.

(17) Ohzuku, T.; Ueda, A. Solid-State Redox Reactions of $LiCoO_2$ ($R\bar{3}m$) for 4 Volt Secondary Lithium Cells. *J. Electrochem. Soc.* **1994**, *141* (11), 2972–2977.

(18) Amatucci, G. G.; Tarascon, J. M.; Klein, L. C. CoO2, The End Member of the Li_xCoO_2 Solid Solution. *J. Electrochem. Soc.* **1996**, *143* (3), 1114–1123.

(19) Ven, A. V. der; Aydinol, M. K.; Ceder, G. First-Principles Evidence for Stage Ordering in Li_xCoO_2. *J. Electrochem. Soc.* **1998**, *145* (6), 2149–2155.

(20) Chen, Z.; Lu, Z.; Dahn, J. R. Staging Phase Transitions in Li_xCoO_2. *J. Electrochem. Soc.* **2002**, *149* (12), A1604–A1609.

(21) Xia, H.; Lu, L.; Meng, Y. S.; Ceder, G. Phase Transitions and High-Voltage Electrochemical Behavior of $LiCoO_2$ Thin Films Grown by Pulsed Laser Deposition. *J. Electrochem. Soc.* **2007**, *154* (4), A337–A342.